Land-Atmosphere Energy Transfer and Surface Boundary Layer Characteristics in the Rongbu Valley on the Northern Slope of Mt. Everest

Authors: Zhong, Lei, Ma, Yaoming, Su, Zhongbo, Lu, Lixin, Ma, Weiqiang, et al.

Source: Arctic, Antarctic, and Alpine Research, 41(3) : 396-405

Published By: Institute of Arctic and Alpine Research (INSTAAR), University of Colorado

URL: https://doi.org/10.1657/1938-4246-41.3.396

Arctic, Antarctic, and Alpine Research, Vol. 41, No. 3, 2009, pp. 396–405

Land-Atmosphere Energy Transfer and Surface Boundary Layer Characteristics in the Rongbu Valley on the Northern Slope of Mt. Everest

*Lei Zhong**†‡$
*Yaoming Ma**§
Zhongbo Su†
Lixin Lu§#
Weiqiang Ma@ and
*Yaqiong Lu**

*Institute of Tibetan Plateau Research, Chinese Academy of Sciences, P.O. Box 2871, No. 18, Shuangqing Road, Beijing 100085, China
†Department of Water Resources, International Institute for Geo-Information Science and Earth Observation, Hengelosestraat 99, Enschede, VV 7500 AA, Netherlands
‡Lanzhou Institute of Arid Meteorology, China Meteorological Administration, No. 2070, Donggang East Road, Lanzhou, Gansu 730020, China
§School of Geography and Remote Sensing, Beijing Normal University, No. 19, Xinjiekou Wai Street, Beijing 100875, China
#Department of Atmospheric Science, Colorado State University, Fort Collins, Colorado 80523, U.S.A.
@Cold and Arid Regions Environmental and Engineering Research Institute, Chinese Academy of Sciences, No. 320, Donggang West Road, Lanzhou, Gansu 730000, China
$Corresponding author: lei@itc.nl

DOI: 10.1657/1938-4246-41.3.396

Abstract

The land-atmosphere interaction processes are unique at Mt. Everest as a result of high elevation. Based on turbulent data collected from April 2005 to March 2006 with the eddy covariance method at Quzong in the Rongbu Valley on the northern slope of Mt. Everest, land-atmosphere energy budget before and after the southwest monsoon onset and surface layer turbulent characteristics are studied for the first time. It is found that energy budget components (net radiation flux, sensible heat flux, latent heat flux, and soil heat flux) and surface heating field have strong diurnal and seasonal variations. In particular, under the influence of the southwest monsoon, the characteristics of surface parameters can be clearly identified. From pre-monsoon to monsoon season, the sensible heat flux decreases whereas the latent heat flux increases. The latent heat flux and Evaporative Fraction at Quzong are relatively high most of the year. Furthermore, the intensity of heating source in the wet season (from June to August) is much greater than that in the dry season (from October to December). The relationship between normalized standard deviation of wind speed and atmospheric stability, variations of normalized standard deviation of temperature, and humidity with atmospheric stability are analyzed using the Monin-Obukhov similarity theory. The result reveals that the normalized standard deviation of velocity components of the three-dimensional wind speed follows similarity relationships in the convective and near-neutral surface layer, but does not seem to be valid in stable surface layer. However, the normalized standard deviation of temperature and humidity does not obey Monin-Obukhov similarity theory in the entire interval of atmospheric stratifications.

Introduction

Located at the western part of China, with an average elevation of more than 4000 m above sea level, the Tibetan Plateau makes up approximately one-fourth of the land area of China. The dynamical and thermal dynamical effects, together with the energy transfer and mass exchange between land surface and atmosphere on the Tibetan Plateau, greatly influence the climate over China, East Asia, and even over the globe. The parameterization schemes of global and regional climate models for the Plateau can only be examined and improved by first observing the physical processes of the land-atmosphere system and determining the characteristics of turbulent parameters, such as turbulent intensity, sensible heat flux, and latent heat flux. In many field experiments conducted since the 1950s, such as the Qinghai-Xizang Plateau Meteorology Experiment (QXPMEX), the Tibetan Plateau Experiment of Atmospheric Sciences (TIPEX), the GEWEX Asian Monsoon Experiment over the Tibetan Plateau (GAME-Tibet) and the Coordinated Enhanced Observing Period Asian-Australia Monsoon Project on the Tibetan Plateau (CAMP-Tibet), a large amount of valuable data have been collected, and abundant scientific results have been obtained (e.g. Bian et al., 2003; Choi et al., 2004; Gao et al., 2000; Hong et al., 2004; Ma and Tsukamoto, 2002; Ma et al., 2002, 2005; Tanaka et al., 2001; Tsukamoto et al., 1995; Ye and Gao, 1979; Zhou et al., 2000). However, the special geographical environment and extreme climatic conditions on the Tibetan Plateau make the field observations very difficult and many experiments were only conducted near the cities and in some regions with relatively convenient transportation. Consequently, no field experiments took place in the most challenging areas near the Himalayas.

The mountainous Mt. Everest region has few residents and is difficult to access. Therefore, it is an optimal area to observe the natural atmospheric environment. The structure of the atmospheric boundary layer over flat, homogeneous surfaces under a

1523-0430/09 $7.00

TABLE 1

Seasonal variations of air temperature, relative humidity, wind speed, and air pressure at Quzong.

Time(month)	4	5	6	7	8	9	10	11	12	1	2	3	Annual mean
Air temperature (°C)	4.1	5.8	10.6	11.4	11.5	8.3	2.6	−2.4	−2.8	−4.4	−1.6	−1.7	3.5
Relative humidity (%)	48	42.4	54.5	67.8	68.9	65.5	50.1	29.4	15.1	19.2	23.6	35	43.3
Wind speed (m s^{-1})	4.0	4.3	3.5	2.7	2.7	4.3	3.9	4.3	6.7	5.8	4.5	4.3	4.3
Air pressure (hPa)	589	590	590	592	591	577	588	590	588	587	590	588	588

range of atmospheric conditions is well understood through various observational experiments. However, there are large uncertainties about the surface layer over complex terrain. Existing experimental studies have reported inconsistent results; therefore, additional data in complex terrain are needed to help understand the structure of surface boundary layer in such areas. In this paper, we report for the first time one-year turbulent data and analysis for the energy and mass exchanges on the northern slope of Mt. Everest.

Taylor (1935) first applied statistical methods in the study of turbulent structure. Since then great advances have been made in turbulent theories such as spectra concept, turbulent scale concept, turbulent variance intensity, etc. A successful example of study on turbulent structure of the surface layer is the formulation of the similarity theory through dimensional analysis by Monin and Obukhov (1954). The concept of Monin-Obukhov (MO hereafter) length (L) was also introduced and the relationship between wind speed and MO length (L) was built according to dimensional analysis. As proposed by MO, various atmospheric parameters and statistics, when normalized by appropriate powers of scaling velocity (u_*), scaling temperature (T_*), and humidity (q_*), become universal functions of a stability parameter (z/L). Field experiments have been conducted to verify the validity of the Monin-Obukhov Similarity theory (MOS hereafter) under stable and unstable conditions in terms of meteorological data. Results show that the MOS hypothesis is not always valid. For example, Mahrt et al. (1998) found that under a very stable regime MOS tends to break down. In this paper, we will examine the MOS against our observations. Quantitative descriptions of the surface boundary-layer characteristics on the northern slope of Mt. Everest will also be provided.

Field Experiment, Instrumentation, and Data Processing

In April 2005, an observation station of the Chinese Academy of Sciences was built in the Mt. Everest area. The field experiment is near a village named Quzong in the Rongbu valley, on the northern slope of Mt. Everest. The site is at 28.310°N, 86.896°E with an elevation of 4475 m above sea level, 24.5 km northeast of the Mt. Everest Base Camp. The land cover is classified as alpine river valley grassy marshland (grass height of about 5 cm) and this region belongs to a temperate monsoon climate zone. The annual mean air temperature was about 3.5°C with annual mean relative humidity of 43.3%, wind speed of 4.3 m s^{-1}, and surface pressure of 588 hPa during the experiment period from April 2005 to March 2006 (Table 1). Based on the data collected from 1966 to 1968 in the Mt. Qomolangma area, Zheng (1975) derived that the annual mean precipitation in this area was only about 225 mm, among which the precipitation from June to September made up to 96%. The annual evaporation was 2319 mm. Table 1 shows that there is a clear increasing trend of relative humidity together with decreasing wind speed during the monsoon season (from June to August). As can be seen in Figure 1, the site location is in a valley which has a west-east orientation at the observation site. The experiment area is relatively flat and open. It is about 1 km in the east-west direction and 6 km in the north-south direction (Fig. 1).

The instrumentation is an eddy covariance (EC) system. It consists of a data logger (CR5000), sonic anemometer (CSAT3), CO_2 and H_2O gas analyzer (LI7500), and a PC card of 1 GB. The data logger CR5000 with a memory of 2 MB controls the measurement, calculation, and data storage. CSAT3 measures three-dimensional wind field and air temperature. LI7500 measures concentrations of CO_2 and H_2O. The measurements of CSAT3 and LI7500 are exported in SDM. The measurement system calculates fluxes online and stores the fluxes and time series data. Other sensors include a temperature and relative humidity probe (HMP45C), a heat flux plate (HFP01), and a set of four-component radiometers made in The Netherlands (Kipp & Zonen; CNR-1). LI7500, CSAT3, and HMP45C were installed at 3 m above the ground. CNR-1 was 1.5 m above the ground, and the soil heat flux plate was installed horizontally at 10 cm below land surface.

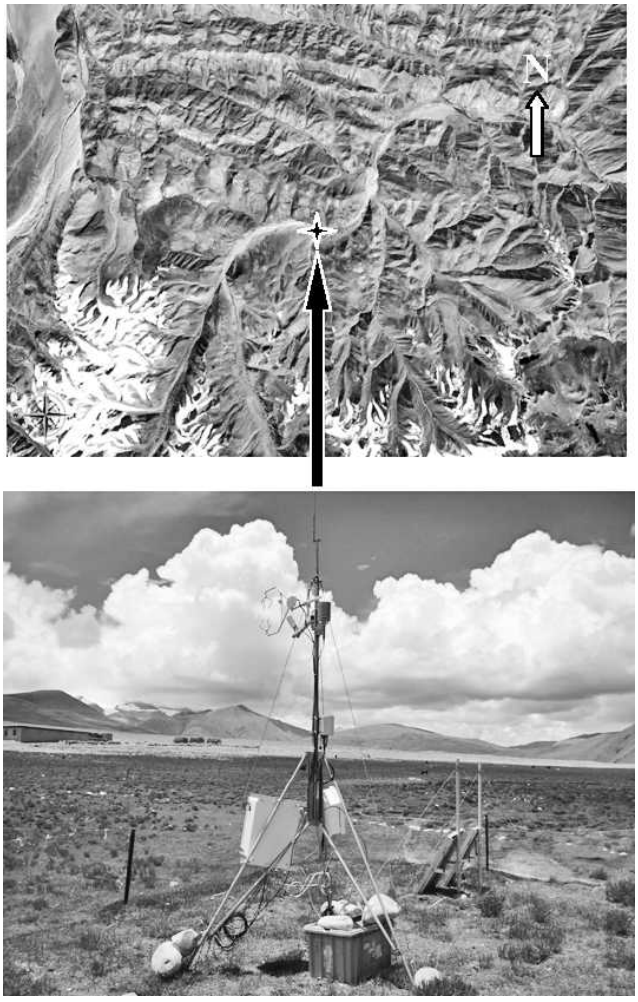

FIGURE 1. The eddy covariance (EC) system at Quzong.

The data sampling of the turbulent observation system was set at a frequency of 10 Hz without interruption. One year of consecutive observation under different atmospheric conditions at Quzong site was conducted from April 2005 through March 2006. We selected 30-minute intervals to calculate the turbulent statistics. Several processing techniques including despiking, gap-filling, and Webb-Pearman-Leuning (WPL) correction were applied to the eddy covariance data. The major data quality control systems are (1) identification of spikes following the methods of Vickers and Mahrt (1997); (2) as there were not very large gaps, linear interpolation method to interpolate the missing values; and (3) density correction of scalar fluxes after Webb et al. (1980). To ensure the data quality, the following data were also excluded (Zhang et al., 2004): (1) when average wind speed is lower than 1.5 m s^{-1}; (2) when friction velocity (u_*) is lower than 0.05 m s^{-1}.

Eddy covariance method is adopted in the processing of turbulent data. Main calculating formulas are as follows:

Three dimensional wind speed fluctuation:

$$u' = u - \overline{u},\ v' = v - \overline{v},\ w' = w - \overline{w} \tag{1}$$

Characteristic frictional velocity: $$u_* = \left(\left(\overline{u'w'}\right)^2 + \left(\overline{v'w'}\right)^2 \right)^{1/4} \tag{2}$$

Characteristic temperature: $$T_* = -\frac{\overline{\theta' w'}}{u_*} \tag{3}$$

Characteristic specific humidity: $$q_* = -\frac{\overline{w'q'}}{u_*} \tag{4}$$

Monin-Obukhov length: $$L = -u_*^3 \Big/ \left(\kappa \frac{g}{\overline{\theta}} \overline{\theta' w'} \right) \tag{5}$$

Wind fluctuating standard deviation:

$$\sigma_u = \sqrt{\overline{u'u'}},\ \sigma_v = \sqrt{\overline{v'v'}},\ \sigma_w = \sqrt{\overline{w'w'}} \tag{6}$$

Turbulent intensity: $$I_u = \frac{\sigma_u}{u_*},\ I_v = \frac{\sigma_v}{u_*},\ I_w = \frac{\sigma_w}{u_*} \tag{7}$$

Sensible heat flux: $$H_s = \rho C_p \overline{\theta' w'} \tag{8}$$

Latent heat flux: $$\lambda E = L_v \rho \overline{w'q'} \tag{9}$$

where u, v, and w (m s^{-1}) are three-dimensional instantaneous wind speed measured by sonic anemometer; $\bar{u}$, $\bar{v}$, and $\bar{w}$ are three-dimensional average wind speed. θ (K) and ρ (kg m^{-3}) are potential temperature and air density, respectively, and they are acquired by calculating simultaneous air pressure and temperature; κ is von Karman constant ($\kappa = 0.4$), g is gravity acceleration ($g = 9.8$ m s^{-2}), C_p is the specific heat of air at constant pressure ($C_p = 1005$ J·kg^{-1}·K^{-1}), and L_v is the latent heat of vaporization ($L_v = 2.257$ MJ·kg^{-1}).

Results and Discussion

THE CHARACTERISTICS OF SURFACE ENERGY BUDGET AND SURFACE HEATING FIELD

Surface Energy Budget

Based on the atmospheric observation data at Quzong from April 2005 to March 2006, isoline maps of monthly mean of half-hourly distribution of energy budget components are drawn (Fig. 2). The radiation flux directed toward the surface is positive, while other energy fluxes directed away from the surface are positive. The figure shows the net radiation flux, sensible heat flux, latent heat flux, and soil heat flux have evident diurnal and seasonal cycles. Generally speaking, along with the increasing of solar elevation after sunrise, the energy budget components increase gradually and reach their maximum between 14:00 and 16:00 (Beijing Standard Time [BST hereafter]; BST is 2 h earlier than local time). Then, they decrease with the decreasing of solar elevation and become negative after sunset. The isolines are much sparser at nighttime indicating that the variation of energy fluxes is much smaller at nighttime than at daytime. As for the seasonal changes of net radiation flux (Fig. 2a), the high value center (more than 500 W m^{-2}) occurs during the summer (from April to September). The highest value is 635 W m^{-2} occurring at 14:00 (BST) in the afternoon of July, and the lowest value is -135 W m^{-2} appearing at 20:00 (BST) in November. The maximum and minimum of net radiation flux represent the timing of receiving and losing largest energy at the land surface, respectively. Under the influence of the southwest monsoon which broke out from the end of May and the beginning of June, the sensible heat flux and latent heat flux on the northern slope of Mt. Everest have opposite variation trends. The daytime sensible heat flux at Quzong experiences a "high-low-high" pattern. It decreases from pre-monsoon to monsoon period before it increases again from monsoon to post-monsoon period (Fig. 2b). In the pre-monsoon period of May, a high value center of sensible heat flux occurs with a maximum of 167 W m^{-2}. During the monsoon season (from June to August), sensible heat flux decreases gradually and has an increasing trend after the monsoon. Another high value (more than 190 W m^{-2}) occurs during daytime in March of the following year. Two nighttime low value centers occur in December with the minimum of -74 W m^{-2} at 3:00 (BST) and -82 W m^{-2} at 19:30 (BST). This is due to the nighttime radiative cooling of the land surface causing a rapid decrease of surface temperature and resulting in a negative temperature gradient between the surface and the air above it. With onset of the monsoon, there are two daytime high value centers of latent heat flux in June and August, respectively (Fig. 2c). The center values are 468 W m^{-2} and 438 W m^{-2} and occur at 15:00 (BST) and 16:00 (BST) in the afternoon. The strong solar radiation and high soil water content at this time lead to high evaporation and make the high latent heat flux centers occur. The latent heat flux decreases in the post-monsoon period and rises again from January to March in the following year. The variation of soil heat flux is smoother in general. One daytime high value center and two nighttime low value centers occur in September with the center value of 342 W m^{-2}, -130 W m^{-2}, and -143 W m^{-2}, respectively (Fig. 2d). This indicates there is a positive soil temperature gradient in the daytime and a negative gradient during the nighttime.

Surface Heating Field

The surface heating effects of the Tibetan Plateau on the overlaying atmosphere have important influence on the weather and climate variations in the eastern part of China and eastern Asia. The surface heating effects of the Tibetan Plateau are determined by turbulent and radiation processes. The quantity of $R_n - G$ represents surface heating intensity, where R_n is net radiation and, G is soil heat flux. When $R_n - G > 0$, heat energy is transferred from the land surface to the atmosphere above, and the land surface is the heating source to the atmosphere. While $R_n - G < 0$, the underlying surface is the heat sink of the atmosphere. As illustrated in Figure 3, the land surface of Quzong is a strong heating source in the day and its heating effects on the atmosphere

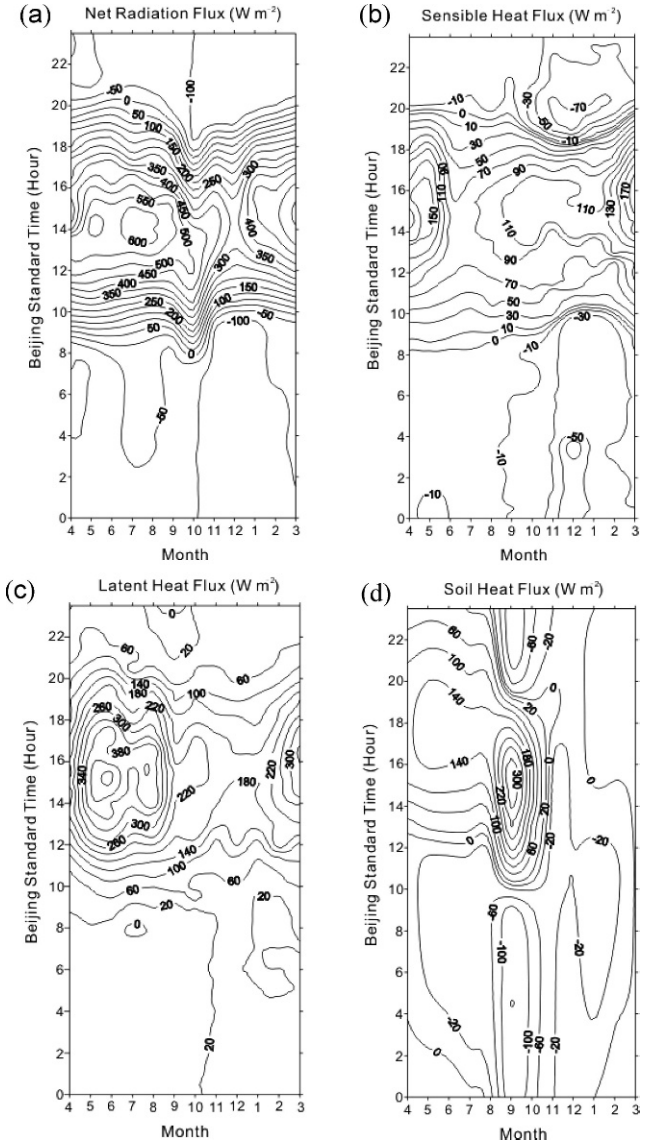

FIGURE 2. Monthly mean of half-hourly distribution of energy budget components. (a) Net radiation flux. (b) Sensible heat flux. (c) Latent heat flux. (d) Soil heat flux. Time span is from April 2005 to March 2006.

are evident. After sunrise in the morning, the surface heating field intensifies gradually and reaches the maximum around 14:00 (BST). Then the surface heating field wears off and changes into a weak cold sink after sunset. The diurnal variation of surface heating intensity in the Tibetan Plateau is determined by the total radiation diurnal variations. At Quzong, the intensity of the heating source in the wet season (from June to August) is much greater than that in the dry season (from October to December). Two high value centers occur during the monsoon season and post-monsoon season. The peak values of the two centers are 566 W m^{-2} and 463 W m^{-2}, respectively.

THE DIURNAL AND SEASONAL BEHAVIOR OF SURFACE PARAMETERS

Energy Budget Components

To show diurnal and seasonal progression of the energy budget components and their variation characteristics before and after the onset of the monsoon, the data on typical sunny days (29

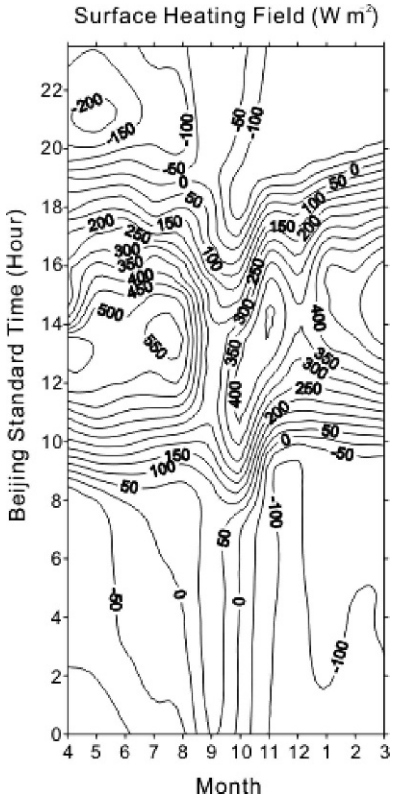

FIGURE 3. Variation characteristics of surface heating field ($R_n - G$) at Quzong. Time span is from April 2005 to March 2006.

April, 22 October, 12 December) and one day—23 July—in the monsoon season are chosen. As can be seen from Figure 4, net radiation flux, sensible heat flux, latent heat flux, and soil heat flux show clear diurnal variation. The energy budget components ascend with increasing solar elevation after sunrise. They reach the maximum around noon, then decrease gradually with decreasing solar elevation. There are clear lag effects between net radiation flux and the other three fluxes, which reflect that net radiation flux variation is the base of sensible heat flux, latent heat flux, and soil heat flux variation. From summer (Fig. 4b) to winter (Fig. 4d), the net radiation flux received by the land surface decreases gradually. The soil heat flux descends from a diurnal average value of 30 W m^{-2} in summer (Fig. 4b) to -12 W m^{-2} in winter (Fig. 4d). And the diurnal variation of soil heat flux appears to be S-shaped, except in winter when it fluctuates around zero. In the pre-monsoon period (Fig. 4a), the land surface is relatively wet and the diurnal average value of latent heat flux (109 W m^{-2}) is larger than that of sensible heat flux (62 W m^{-2}). The Bowen ratio is 0.57 and soil heat flux takes up 20.3% of the net radiation flux. After the onset of the monsoon (Fig. 4b), influenced by precipitation, the land surface becomes wetter and the average value of the latent heat flux (113 W m^{-2}) is much higher than that of the sensible heat flux (21 W m^{-2}). However, because of the cloudy weather in the monsoon season, there is little decrease of the net radiation flux and soil heat flux. The soil heat flux takes up 17.2% of the net radiation flux. The Bowen ratio decreases further to 0.19. In the post-monsoon period (Fig. 4c), the latent heat flux decreases and the sensible heat flux increases at the same time. However, the latent heat flux (84 W m^{-2}) is still larger than the sensible heat flux (34 W m^{-2}) with Bowen ratio about 0.4. The soil heat flux decreases greatly and takes up only 5% of the net radiation flux. In December (Fig. 4d), the latent heat flux reduces

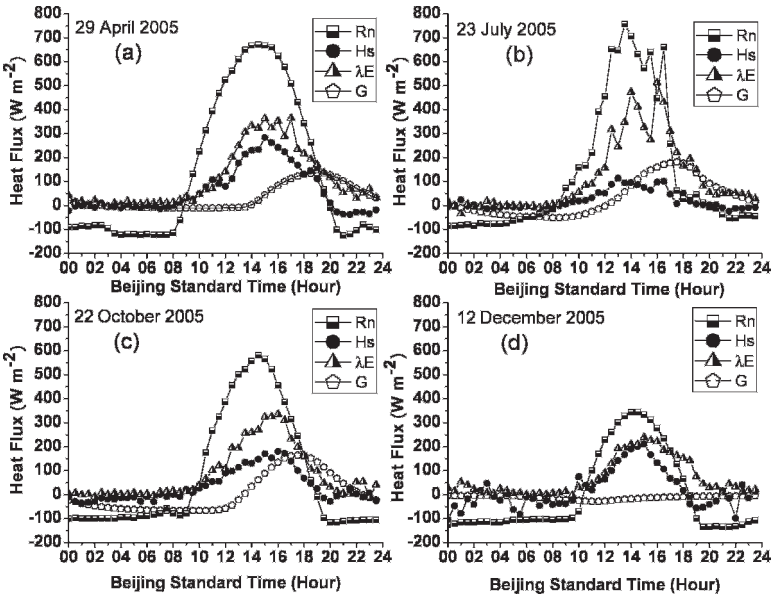

FIGURE 4. Diurnal and seasonal variation of the energy budget components on four typical days in different seasons. (a) Spring. (b) Summer. (c) Autumn. (d) Winter. R_n = net radiation flux, H_s = sensible heat flux, λE = latent heat flux, G = soil heat flux.

further to the same level as the sensible heat flux. In summary, the latent heat flux at Quzong is relatively high most of the year. This is, in part, due to the moist underlying surface of valley grassy marshland, and the high water content in the soil.

It must be pointed out that imbalance of the energy budget is also found in our study area. The energy balance ratio which is defined as $(H_s + \lambda E)/(R_n - G)$ is calculated at a monthly interval using the observational data sets. It equals 0.92 which is not perfect, but acceptable. Several reasons may account for the surface energy imbalance phenomenon: (1) eddy covariance estimates of $H_s + \lambda E$ are too low because low frequency, large scale atmospheric motions are undersampled by half-hourly eddy covariance flux measurements; (2) horizontally advected energy is not measured and it may be large enough to cause some imbalance; (3) measurements of G are a little lower than its actual value because the heat storage between the land surface to 10 cm depth was not included in the calculation of G.

Evaporative Fraction

The Evaporative Fraction (*EF*), which characterizes the partition of the surface energy budget, is defined as the ratio between the latent heat flux and available energy at the surface.

$$EF = \frac{\lambda E}{H_s + \lambda E} \tag{10}$$

The diurnal behavior of *EF* in different seasons is presented in Figure 5. It can be seen that for the Quzong site, *EF* exhibits a typical concave-up shape from 8:00 to 20:00 BST. *EF* increases sharply at sunrise and sunset because the available energy that appears in the denominator of *EF* changes most rapidly at those periods. Due to the small variation of available energy and consistent supply of soil water, the changing trend of *EF* is relatively small at other times, especially around 14:00 BST. Table 2 shows some particular variation characteristics of sensible heat flux, latent heat flux, and *EF* at three other sites in the Tibetan Plateau. In the pre-monsoon period of April, the sensible heat flux at Quzong is the lowest while latent heat flux is the highest among the four sites. The latent heat flux (75 W m^{-2}) of Quzong in the pre-monsoon season is even much higher than those of Damxung (50 W m^{-2}) and Gerze (41 W m^{-2}) in the monsoon season. The *EF* at this time period is 0.66 and it is much higher than those of other sites. This suggests that the local environment of Quzong (e.g. sufficient supply of soil water) may change the seasonal distribution of energy fluxes and make it different from other sites which are mainly influenced by the monsoon climate. The *EF* at Quzong increases to a much higher value of 0.85 from the pre-monsoon season to the monsoon season.

TURBULENT STATISTICAL CHARACTERISTICS

The Relationship between Normalized Standard Deviation of Wind Speed and Atmospheric Stability

Researchers have given much attention for many years to the study of the correlation between wind velocity components, temperature variation, and atmospheric stability. The results of Arya and Sundararajan (1976) show that the horizontal wind standard deviation, after normalized by friction velocity, would increase with the rising of atmospheric stability under unstable conditions. Panofsky et al. (1977) found the following relationships hold above the flat underlying surface under convective conditions:

$$\sigma_u/u_* \approx \sigma_v/u_* = (12 - 0.5z/L)^{1/3} \tag{11}$$

$$\sigma_w/u_* = 1.3(1 - 3z/L)^{1/3} \tag{12}$$

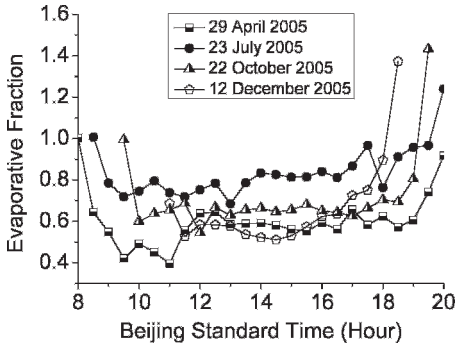

FIGURE 5. Diurnal evolution of *EF* in different seasons at Quzong.

TABLE 2

Comparison of monthly mean turbulent heat fluxes and Evaporative Fraction (*EF*) of different sites in the Tibetan Plateau from pre-monsoon (April or May) to monsoon season (July).

Site	Elevation (m)	Latitude (°N)	Longitude (°E)	Period	H_s (W m^{-2})	λE (W m^{-2})	*EF*	Source
Gerze	4200	32.22	84.8	May	46	11	0.19	Bian et al.(2003)
				July	44	41	0.48	
NPAM	4620	31.93	91.72	April	63	18	0.22	Zhong (2007)
				July	6	125	0.95	
Damxung	4260	30.03	91.1	May	74	3	0.04	Bian et al.(2003)
				July	58	50	0.46	
Quzong	4475	28.31	86.9	April	39	75	0.66	This paper
				July	21	121	0.85	

After normalization by friction velocity, the three-dimensional standard deviation of wind fluctuation should relate with stability parameters: $\sigma_u/u_* = \Phi_u(z/L)$, $\sigma_v/u_* = \Phi_v(z/L)$, $\sigma_w/u_* = \Phi_w(z/L)$. According to MOS, under near neutral conditions ($z/L \approx 0$), the turbulence in the atmospheric surface layer is mainly caused by mechanical movements. Hence, all the similarity functions should be constant. That means $\sigma_u/u_* = A$, $\sigma_v/u_* = B$, and $\sigma_w/u_* = C$, in which A, B, and C are constants.

In order to study the possible effects of the topography on the turbulent characteristics, the data collected at Quzong are grouped into two categories. The first one has time series with wind directions of $90^\circ \pm 45^\circ$ and $270^\circ \pm 45^\circ$. These data are referred to as along-the-valley. The second one has other wind directions which are called cross-the-valley.

As can be seen in Figures 6a, 6c, and 6e for along-the-valley, parallel wind directions, the relationships between the normalized standard deviation of three-dimensional wind speed and $-z/L$ follow the ''law of 1/3 power'' for the unstable conditions at the Quzong site of Mt. Everest. The optimal similarity functions are as follows:

$$\sigma_u/u_* = \Phi_u(z/L) = 3.55(1-0.72z/L)^{1/3} (0.001 < -z/L < 10) \quad (13)$$

$$\sigma_v/u_* = \Phi_v(z/L) = 3.12(1-4.53z/L)^{1/3} (0.001 < -z/L < 10) \quad (14)$$

$$\sigma_w/u_* = \Phi_w(z/L) = 0.98(1-5.14z/L)^{1/3} (0.001 < -z/L < 10) \quad (15)$$

Under neutral atmospheric conditions, σ_u/u_*, σ_v/u_*, and σ_w/u_* tend to become constant (A = 3.55, B = 3.12, C = 0.98). The horizontal and vertical turbulent intensity increases with the strengthening of atmospheric instability. For transverse wind directions (Figs. 7a, 7c, and 7e), $\sigma_i/u_*(i = u,v,w)$ also has some dependence with $-z/L$ for the unstable conditions, and the optimal fitting functions are given by

$$\sigma_u/u_* = \Phi_u(z/L) = 3.52(1-2.21z/L)^{1/3} (0.001 < -z/L < 10) \quad (16)$$

$$\sigma_v/u_* = \Phi_v(z/L) = 3.16(1-5.63z/L)^{1/3} (0.001 < -z/L < 10) \quad (17)$$

$$\sigma_w/u_* = \Phi_w(z/L) = 0.91(1-7.42z/L)^{1/3} (0.001 < -z/L < 10) \quad (18)$$

The increasing trends of $\sigma_i/u_*(i = u,v,w)$ with increasing unstable conditions can be seen from Figures 6a, 6c, 6e, 7a, 7c, and 7e, which are mainly due to the increase in the magnitude of σ_i under convective conditions. Equations 13–18 show that the turbulence has some similar relationships for parallel and transverse wind conditions, which means that although the Quzong site is in a valley, the topography there has little influence on the transverse wind flows. This is because the relatively high elevation of the observation site, and the homogeneous surface layer of short grass satisfy the precondition of MOS. The valley is also quite wide, which allows transverse wind flows to adjust to local equilibrium by the time they reach the sensor.

On the other hand, under stable atmospheric boundary layer conditions, it is still not clear whether MO similarity relationships between $\sigma_i/u_*(i = u,v,w)$ and z/L exist. Mahrt et al. (1998) thought such relationships do not exist under stable conditions. However, Anfossi et al. (2005) considered there is a certain relationship under stable conditions. As shown by Figures 6b, 6d, 6f, 7b, 7d, and 7f, under both the parallel and transverse wind directions, due to the significant decrease of u_*, $\sigma_i/u_*(i = u,v,w)$ increase with the increasing stability. However, the observational data are so scattered that they prevent us from deriving any particular function, which means MOS may not be appropriate in describing the turbulence characteristics. Several reasons may account for this phenomena as described by Mahrt (1999). First, the strong stability makes a traditional surface layer non-existent. Second, possibility is that the surface layer exists but is below the observational level as that indicated by Haugen et al. (1971) and Howell and Sun (1999). Third, the turbulence and stability functions cannot be adequately measured because of instrumental and flux sampling problems in weak intermittent turbulence.

Therefore, although the observation site is in a valley, evidence is shown that the MOS is not only applicable to horizontal wind variations but also to vertical wind variations under unstable conditions. In spite of the difference in coefficients from other regions, the law of 1/3 power between $\sigma_i/u_*(i = u,v,w)$ and $-z/L$ is confirmed. As for the stable condition, MOS is not valid in our experiment area.

The Variations of Normalized Standard Deviation of Temperature and Humidity with Atmospheric Stability

The general relationship between non-dimensional standard deviation of temperature, humidity, and atmospheric stabilities can be described as follows:

$$\sigma_T/|T_*| = \alpha(-z/L)^{-1/3} \quad (19)$$

$$\sigma_q/|q_*| = \beta(-z/L)^{-1/3} \quad (20)$$

where α and β are constants.

Non-dimensional standard deviation of temperature ($\sigma_T/|T_*|$) and humidity ($\sigma_q/|q_*|$) are plotted with z/L, respectively, in Figure 8. Under both wind directions, $\sigma_T/|T_*|$ and $\sigma_q/|q_*|$ do not show the tendency to stay constant, but appear to increase as stability approaches zero at the near-neutral conditions for both

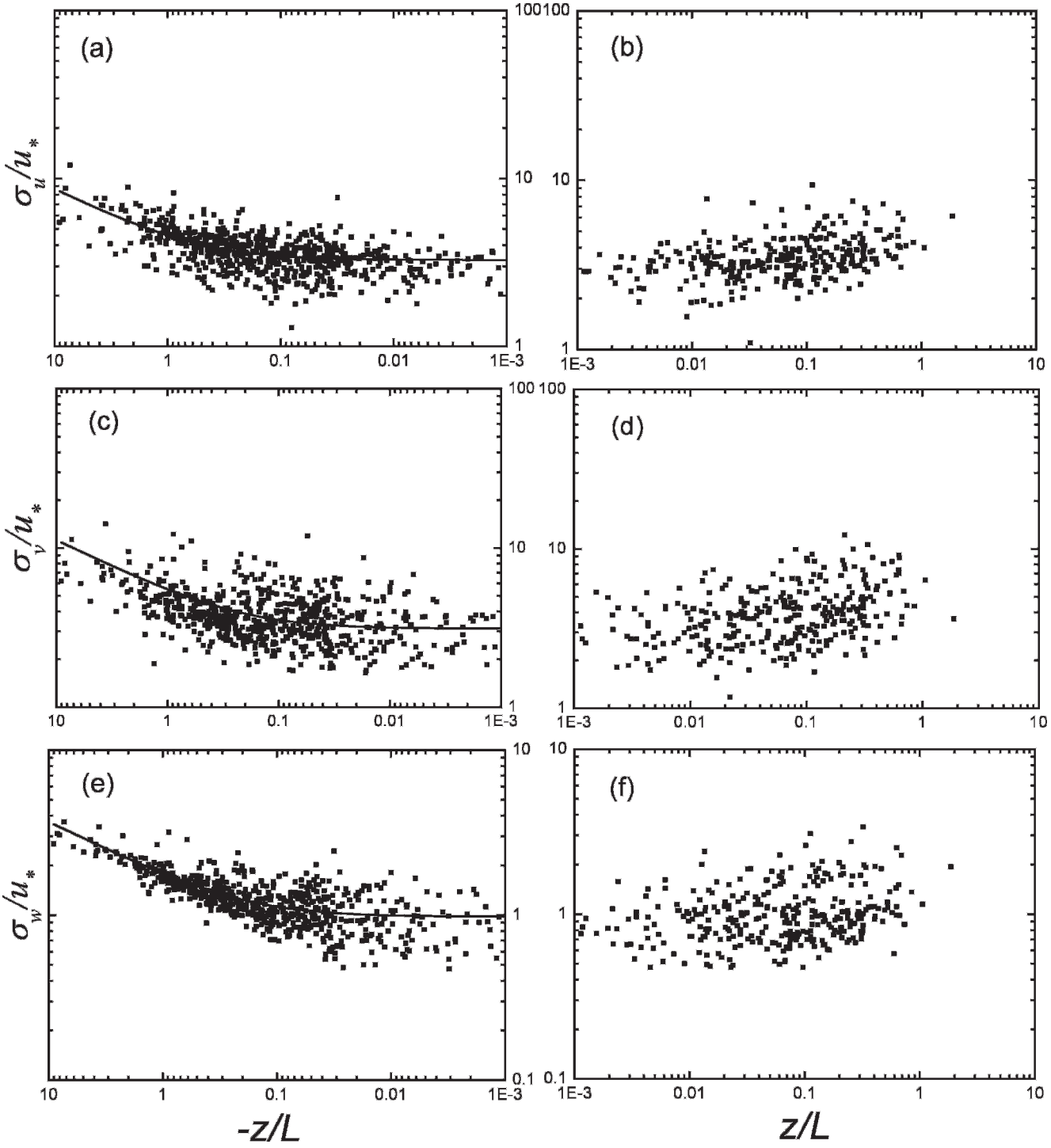

FIGURE 6. Turbulence characteristics of the longitudinal (a, b), lateral (c, d), and vertical velocity (e, f) with stability during the monsoon season (from 1 to 31 July) for parallel wind direction (along-the-valley). The left panel (a, c, e) and right panel (b, d, f) show the convective and stable cases, respectively. A total of 977 data points are analyzed in this figure. Line: experimental law; points: observations.

stable and unstable regimes. The reason is that $|T_*|$ and $|q_*|$ approach zero at the neutral point more rapidly than the fluctuations of temperature and humidity. As can also be seen from Figure 8, the dispersion extent of $\sigma_q/|q_*|$ is a little larger than $\sigma_T/|T_*|$. This may be caused by the much greater importance of the large eddies on $\sigma_q/|q_*|$ than $\sigma_T/|T_*|$ at the experimental area. Zhang et al. (2001) reported that the behavior of the scaled standard deviation of temperature and humidity is independent of the observation height and surface conditions. The phenomena of much scattered $\sigma_q/|q_*|$ than $\sigma_T/|T_*|$ is also observed in other studies (Sempreviva and Gryning, 1996; Tamagawa, 1996).

Conclusions

In this paper, the observations of atmospheric surface-layer parameters were carried out at the bottom of an open valley using a set of eddy covariance systems from April 2005 to March 2006. Through observation and calculation of energy budget and

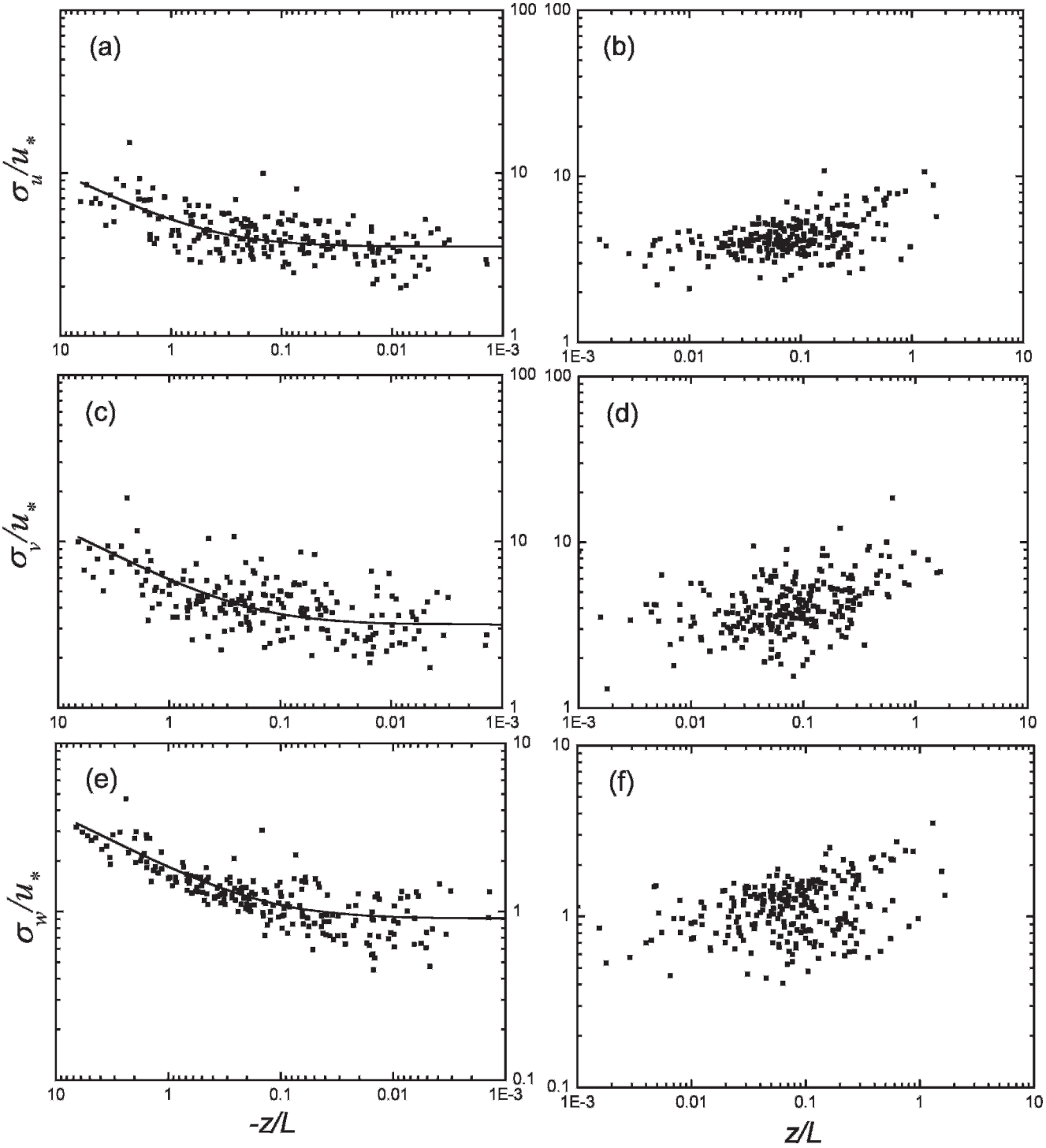

FIGURE 7. Turbulence characteristics of the longitudinal (a, b), lateral (c, d), and vertical velocity (e, f) with stability during the monsoon season (from 1 to 31 July) for transverse wind direction (cross-the-valley). The left panel (a, c, e) and right panel (b, d, f) show the convective and stable cases, respectively. A total of 473 data points are analyzed in this figure. Line: experimental law; points: observations.

atmospheric turbulence on the northern slope of Mt. Everest, diurnal and seasonal land-atmosphere energy transfer characteristics are investigated. The effectiveness of MOS is examined for different wind directions and atmospheric stratifications. The conclusions are drawn as follows.

(1) Energy budget components in Mt. Everest have evident diurnal and seasonal changes. The variation is much smoother in nighttime than in daytime. Under the influence of the southwest monsoon, the sensible heat flux and latent heat flux on the north slope of Mt. Everest have opposite variation trends. The variation of soil heat flux is smoother in general. The land surface of Quzong is a strong heat source in daytime and it changes into a weak cold sink after sunset. As far as seasonal variation is concerned, the heating source intensifies more in the wet season (566 W m^{-2}) than that in the dry season (463 W m^{-2}).

(2) *EF* exhibits a typical diurnal concave-up shape behavior; the seasonal changes are also observed. Under the impact of local environment (strong solar radiation, valley grassy

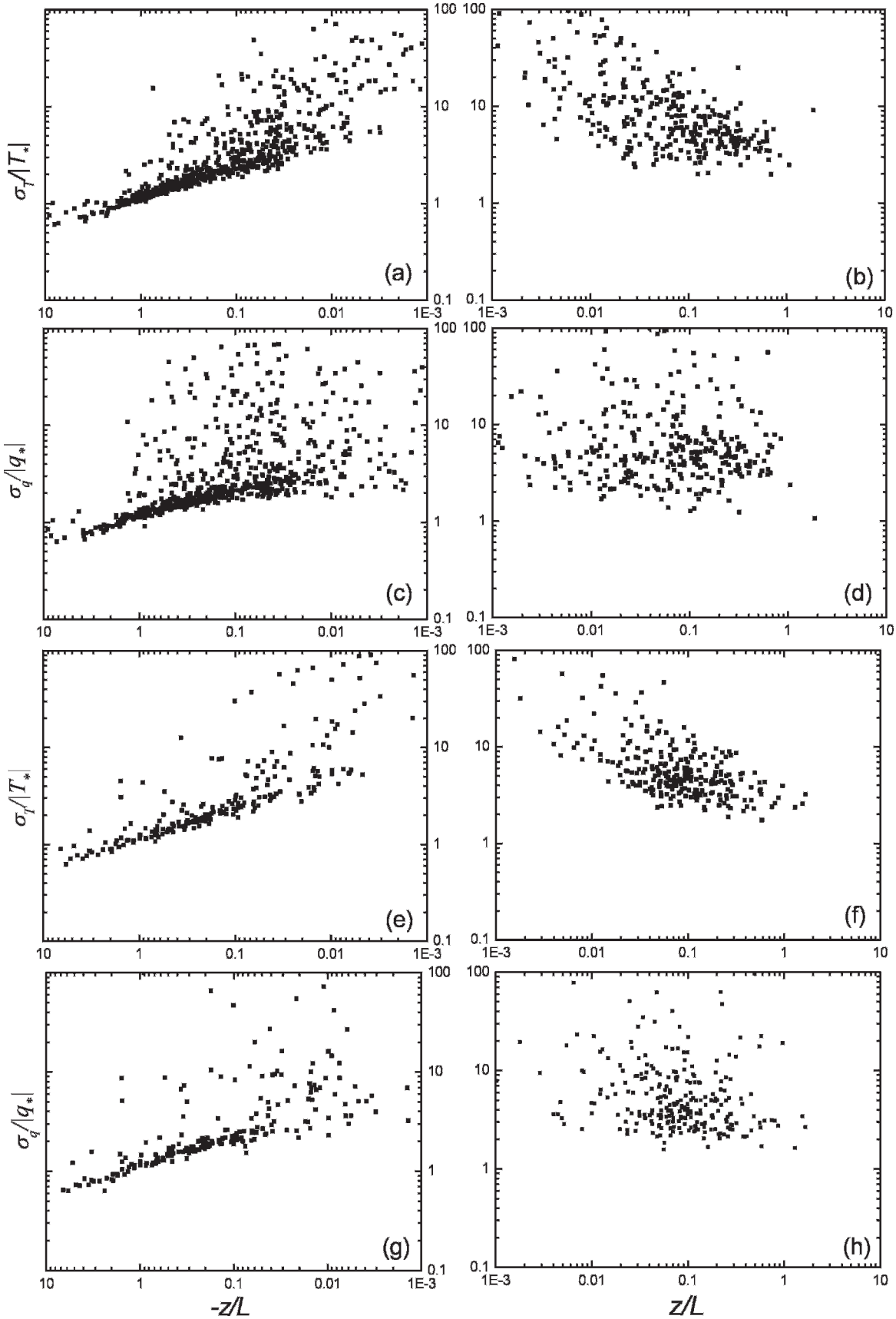

FIGURE 8. Non-dimensional standard deviation of temperature and humidity as a function of stability parameter during the monsoon season (from 1 to 31 July). Upper panels (a, b, c, d) are for parallel wind direction (along-the-valley, 977 data points) and lower panels (e, f, g, h) for transverse wind direction (cross-the-valley, 473 data points).

marshland underlying surface, and abundant water supply in the soil), *EF* is relatively high most times of the year, which indicates the soil of Quzong is very wet and the latent heat exchange between underlying land surface and the above atmosphere is vigorous.

(3) Although the observation site is in a valley, evidence shows that the normalized standard deviation of the velocity components obeys MOS under unstable and near-neutral conditions. The law of 1/3 power between $\sigma_i/u_*(i = u,v,w)$ and $-z/L$ is confirmed. However, MOS does not seem to be valid for the Quzong area under stable stratification.

(4) The normalized standard deviation of temperature and humidity does not obey MOS in the entire interval of z/L studied. However, $\sigma_T/|T_*|$ and $\sigma_q/|q_*|$ appear to increase as stability approaches zero at the near-neutral conditions.

Acknowledgments

This research was financed by the National Natural Science Foundation of China (40825015, 40810059006, and 40705004), Opening Foundation of Institute of Plateau Meteorology, China Meteorological Administration (LPM2006011), and Arid Meteorology Science Foundation of Gansu Provincial Key Laboratory of Arid Climatic Change and Disaster Reduction, Lanzhou Institute of Arid Meteorology, China Meteorological Administration (IAM200810). We are very grateful to anonymous reviewers for their constructive and insightful comments. We also thank all the participants in the field observation for their hard work and cooperation.

References Cited

Anfossi, D., Oettl, D., Degrazia, G., and Goulart, A., 2005: An analysis of sonic anemometer observations in low wind speed conditions. *Boundary-Layer Meteorology*, 114: 179–203.

Arya, S. P. S., and Sundararajan, A., 1976: An assessment of proposed similarity theories for the atmospheric boundary layer. *Boundary-Layer Meteorology*, 10: 149–166.

Bian, L., Xu, X., Lu, L., Gao, Z., Zhou, M., and Liu, H., 2003: Analyses of turbulence parameters in the near-surface layer at Qamdo of the southeastern Tibetan Plateau. *Advances in Atmospheric Sciences*, 20: 369–378.

Choi, T., Hong, J., Kim, J., Lee, H., Asanuma, J., Ishikawa, H., Tsukamoto, O., Gao, Z., Ma, Y., and Ueno, K., 2004: Turbulent exchange of heat, water vapor, and momentum over a Tibetan prairie by eddy covariance and flux variance measurements. *Journal of Geophysical Research–Atmospheres*, 109: article D21106, doi: 10.1029/2004JD004767.

Gao, Z., Wang, J., Ma, Y., Kim, J., Choi, T., Lee, H., Asanuma, J., and Su, Z., 2000: Calculation of near-surface layer turbulent transport and analysis of surface thermal equilibrium features in Nagqu of Tibet. *Physics and Chemistry of the Earth Part B–Hydrology Oceans and Atmosphere*, 25: 135–139.

Haugen, D. A., Kaimal, J. C., and Bradley, E. F., 1971: An experimental study of reynolds stress and heat flux in the atmospheric surface layer. *Quarterly Journal of the Royal Meteorological Society*, 97: 168–180.

Hong, J., Choi, T., Ishikawa, H., and Kim, J., 2004: Turbulence structures in the near-neutral surface layer on the Tibetan Plateau. *Geophysical Research Letters*, 31: doi: 10.1029/2004GL019935.

Howell, J. F., and Sun, J., 1999: Surface-layer fluxes in stable conditions. *Boundary-Layer Meteorology*, 90: 495–520.

Ma, Y., and Tsukamoto, O., 2002: *Combining Satellite Remote Sensing with Field Observations for Land Surface Heat Fluxes over Inhomogeneous Landscape*. Beijing: China Meteorological Press, 172 pp.

Ma, Y., Su, Z., Li, Z., Koike, T., and Menenti, M., 2002: Determination of regional net radiation and soil heat flux over a heterogeneous landscape of the Tibetan Plateau. *Hydrological Processes*, 16: 2963–2971.

Ma, Y., Fan, S., Ishikawa, H., Tsukamoto, O., Yao, T., Koike, T., Zuo, H., Hu, Z., and Su, Z., 2005: Diurnal and inter-monthly variation of land surface heat fluxes over the central Tibetan Plateau area. *Theoretical and Applied Climatology*, 80: 259–273.

Mahrt, L., 1999: Stratified atmospheric boundary layers. *Boundary-Layer Meteorology*, 90: 375–396.

Mahrt, L., Sun, J., Blumen, W., Delany, T., and Oncley, S., 1998: Nocturnal boundary-layer regimes. *Boundary-Layer Meteorology*, 88: 255–278.

Monin, A. S., and Obukhov, A. M., 1954: Basic laws of turbulent mixing in the ground layer of the atmosphere. *Trudy Akad. Nauk S.S.S.R. Geofiz. Inst.*, 24: 163–187.

Panofsky, H. A., Tennekes, H., Lenschow, D. H., and Wyngaard, J. C., 1977: The characteristics of turbulent velocity components in the surface layer under convective conditions. *Boundary-Layer Meteorology*, 11: 355–361.

Sempreviva, A. M., and Gryning, S. E., 1996: Humidity fluctuations in the marine boundary layer measured at a coastal site with an infrared humidity sensor. *Boundary-Layer Meteorology*, 77: 331–352.

Tamagawa, I., 1996: Turbulent characteristics and bulk transfer coefficients over the desert in the HEIFE area. *Boundary-Layer Meteorology*, 77: 1–20.

Tanaka, K., Ishikawa, H., Hayashi, T., Tamagawa, I., and Ma, Y., 2001: Surface energy budget of Amdo on the eastern Tibetan Plateau using GAME/Tibet IOP98 data. *Journal of Meteorological Society of Japan*, 79: 505–517.

Taylor, G. I., 1935: Statistical theory of turbulence. *Proceedings of the Royal Society*, A151: 421–464.

Tsukamoto, O., Sahashi, K., and Wang, J., 1995: Heat-budget and evapotranspiration at an oasis surface surrounded by desert. *Journal of the Meteorological Society of Japan*, 73: 925–935.

Vickers, D., and Mahrt, L., 1997: Quality control and flux sampling problems for tower and aircraft data. *Journal of Atmospheric and Oceanic Technology*, 14: 512–526.

Webb, E. K., Pearman, G. I., and Leuning, R., 1980: Correction of the flux measurements for density effects due to heat and water vapour transfer. *Quarterly Journal of the Royal Meteorological Society*, 106: 85–100.

Ye, D., and Gao, Y., 1979: *Tibetan Plateau Meteorology*. Beijing: Science Press, 278 pp.

Zhang, H., Chen, J., and Park, S. U., 2001: Turbulence structure in unstable conditions over various surfaces. *Boundary-Layer Meteorology*, 100: 243–261.

Zhang, H., Li, F., and Chen, J., 2004: Statistical characteristics of atmospheric turbulence in different underlying surface conditions. *Plateau Meteorology*, 23: 598–604 (in Chinese).

Zheng, D., 1975: The climatic characteristics of nature zone in Mt. Qomolangma area. *In* Scientific Expedition Team to Tibet, Chinese Academy of Sciences (eds.), 1975, *The Scientific Report of Mt. Qomolangma Area Expedition 1966–1968*. Beijing: Science Press, 147–202.

Zhong, L., 2007: Ground measurement and satellite remote sensing of land surface characteristics parameters over the Tibetan Plateau area. Dissertation. Institute of Tibetan Plateau Research, Chinese Academy of Sciences.

Zhou, M., Xu, X., Bian, L., Chen, J., Liu, H., Zhang, H., Li, S., and Zhao, Y., 2000: *Observational Analysis and Dynamic Study of Atmospheric Boundary Layer on Tibetan Plateau*. Beijing: China Meteorological Press, 125 pp.

MS accepted March 2009